Generation of Global Backscatter Maps for Future SAR Missions Design

Luca Dell'Amore[1], José-Luis Bueso-Bello[1], Michele Martone[1], and Paola Rizzoli[1]
[1]Microwaves and Radar Institute, German Aerospace Center (DLR), Wessling, Germany

Abstract

The generation of global backscatter maps allows for the exploitation of a priori knowledge of local synthetic aperture radar (SAR) backscatter statistics. SAR backscatter maps can be used for accurate performance prediction and for the optimization of instrument settings for present and future SAR systems. Also, many further SAR applications can benefit from the availability of backscatter maps in order to monitor the backscatter evolution in time and to investigate the radar reflectivity behaviour depending on sensor parameters and target properties. In this work, X-band backscatter maps are generated by mosaicking images acquired by the TanDEM-X (TDM) mission at global scale. The correction models used for the characterization of backscatter behaviour are based on the database provided by Ulaby in [3] and are here presented for HH polarization and for any required reference incidence angle. As an example of application for future SAR missions design, a novel performance-optimized block-adaptive quantization (PO-BAQ), coming from the need of optimizing the resource allocation of the state-of-the-art quantization algorithms for SAR systems, is then considered. The methodology relies on global backscatter statistics for the generation of bitrate maps, which can provide a helpful information for performance budget definition and for optimizing resource allocation strategies.

1 Introduction

Synthetic aperture radar (SAR) systems represent nowadays a well-recognized technique in the field of remote sensing. They are able to acquire high-resolution images of the Earth's surface, independently of daylight and weather conditions, and provide useful data for a large number of scientific applications, such as hydrology, glaciology, forestry, and oceanography. Precise a priori backscatter knowledge is necessary for an optimized operation of SAR systems in order to automatically adapt radar parameters on-board during a data take. For realistic performance prediction of future SAR systems, the backscatter information represents a valuable input, e.g., for signal-to-noise ratio (SNR) estimation or data clipping values computation. Moreover, many further SAR applications can benefit from the availability of backscatter maps, such as the monitoring of backscatter evolution in time and the investigation of radar reflectivity depending on land type and soil conditions [1]. On the other hand, backscatter maps can also be exploited in the field of quantization. In the last decades, innovative spaceborne radar techniques have been proposed in order to brake the limitations imposed by "conventional" SAR systems and to acquire wider swaths with finer azimuth resolutions. Clearly, the consequent increase in the amount of data implies harder requirements in terms of on-board memory and downlink capacity. This has motivated the investigation of advanced quantization strategies in order to meet a trade-off between the quality of the resulting SAR products and the sensor acquisition capabilities. In this framework, a novel performance-optimized block-adaptive quantization (PO-BAQ) method [2], which exploits the availability of global backscatter maps, has been proposed in order to extend the concept of the state-of-the-art BAQ and to optimize the resource allocation together with the resulting interferometric performance. Large-scale mosaics of backscatter images gain a central role in the generation of SAR backscatter maps and allow for the global monitoring of the Earth's environmental changes as well as the generation of bitrate maps for advanced quantization strategies.

Radar backscattering is defined as the portion of a radar signal which is redirected back to the radar antenna after an interaction with a target on the ground. Its properties depend on several factors, which are related to the instrument itself, such as frequency, polarization, and acquisition geometry, as well as to the characteristics of the illuminated on-ground area, such as soil conditions, surface roughness, and scene topography. Different quantities are usually exploited to represent SAR backscatters, as described in [3] and [4]. However, the radar brightness β^0 is the only one that does not require a precise knowledge of the local incidence angle. In order to avoid mistakes due to limited knowledge of ground topography (which direct impacts on the estimation of the local incidence angle), β^0 will be used in this work as radar backscatter reference quantity.

Several models can be found in the literature to characterize the backscatter behaviour depending on sensor parameters and target properties. Well known and widely used in the scientific community are the ones provided by Ulaby and Dobson in 1989 [3]. Moreover, the availability of a large amount of high-quality SAR data provided by the TanDEM-X (TDM) mission allows for a precise statistical analysis of X-band backscatters from space, depending

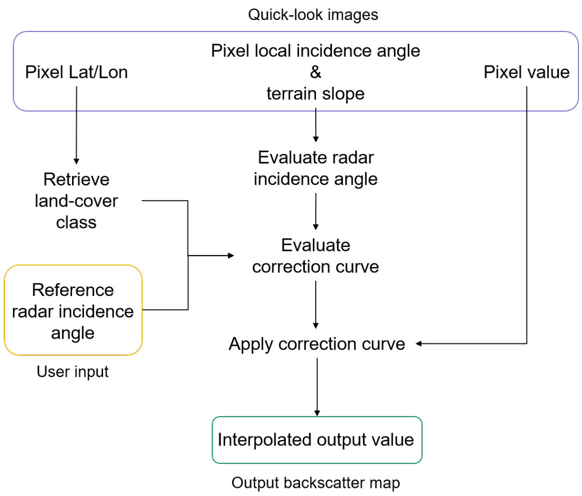

Figure 1 Algorithm flowchart. The output backscatter map is referred to a precise reference radar incidence angle.

on specific system parameters and on-ground target properties, such as polarization, land type, local incidence angle, acquisition and seasonal time [1].

A priori knowledge of global backscatter maps can be thus exploited for accurate performance prediction and for the optimization of instrument settings for present and future SAR systems. This paper is structured as follows. Section 2 shows the procedure for the generation of SAR backscatter maps, focusing on the interpolation algorithm to the output reference radar incidence angle. Section 3 describes the application of the PO-BAQ as example of future quantization enhancement thanks to a priori knowledge of SAR backscatter statistics. Finally, the conclusions are drawn in Section 4.

2 Backscatter Map Generation Algorithm

The objective of this work is the generation of a global X-band backscatter map from TanDEM-X (TDX) quick-look images [5]. Quick-look products are generated as by-pass data by the TanDEM-X operational processor (ITP). They provide less resolution ($\sim$50 x 50 m^2) compared to standard single-look slant-range complex products (SSC Level-1b)[6] and are radiometrically calibrated according to the specified absolute calibration factor. Also, they are geocoded into latitude/longitude coordinates and are provided together with the associated matrix of local incidence angles. The interpolation algorithm is applied depending on the radar range-dependent incidence angle and land-cover class; the output backscatter map has thus to be referred to a precise reference radar incidence angle $\theta_{i,ref}$. The algorithm flowchart is shown in Figure 1. The input β^0 values, associated to different local incidence angles and land-cover classes, are interpolated to a specified output reference radar incidence angle by using the Ulaby backscatter models [3]. In particular, each input β^0 pixel is

Table 1 Mapping the *WorldCover 2020* land-cover map and the land-cover classes of the Ulaby models.

WorldCover 2020	Description	Ulaby model
Tree Cover	Geographic areas dominated by trees (>10%). This class also includes tree covered areas seasonally or permanently flooded with fresh water, except for mangroves.	Trees
Shrubland	Geographic areas dominated by natural shrubs, either evergreen or deciduous (>10%). Shrubs are defined as woody perennial plants with persistent and woody stems (< 5 m).	Shrubs
Mangroves	Intertidal zones of sheltered tropical shores, "overwash" islands, and estuaries, dominated by Salt-tolerant trees.	
Grassland	Geographic areas dominated by natural herbaceous plants without persistent stem and definite firm structure (>10%). It may also contain uncultivated cropland areas (without harvest) in the reference year.	Grasses
Herbaceous wetland	Geographic areas dominated by natural herbaceous vegetation (>10%) that is permanently or regularly flooded by fresh, brackish or salt water.	
Moss and lichen	Geographic areas covered with lichens and/or mosses (no leaves, stems or roots are present).	
Cropland	Geographic areas covered with annual croplands which are sowed/planted and harvestable at least once within the 12 months after the sowing/planting date. The annual cropland is sometimes combined with some tree or woody vegetation.	Short vegetation
Built-up	Geographic areas covered by buildings, roads and other man-made structures. Waste dump deposits and extraction sites are considered as bare.	Roads
Bare/sparse vegetation	Geographic areas with exposed soil, sand, or rocks (<10% vegetated cover during any time of the year).	Soil & Rocks
Snow & ice	Geographic areas covered by snow or glaciers persistently.	Dry snow
Permanent water bodies	Geographic area covered for most of the year (> 9 months) by water bodies.	None

associated to a land-cover class. Many works in the literature relies on the previous *GlobCover* classification map [7], provided by ESA in a resolution of 300 x 300 m^2, for the retrieval of land-cover classes. In this work, the newly released *WorldCover 2020* map at 10 m resolution [8] is used, which provides a better resolution comparable to the quick-look images one. Since the land-cover classes provided by ESA differ from the Ulaby ones, an intermediate step is required in order to associate the *WorldCover* classes with similar statistics to the same Ulaby model. The defined relation between the land-cover classes in both studies is reported in Table 1, with a description of each land-cover class.

The interpolation is performed by evaluating the radar incidence angle θ_i of the β^0 pixel. This can be derived from the local incidence angle θ_{li}, as:

$$\theta_i = \theta_{li} + \alpha \tag{1}$$

where α identifies the terrain slope, which is also provided by the ITP together with the backscatter data and the local incidence angle matrix. A correction factor is thus derived depending on the output reference radar incidence angle $\theta_{i,ref}$ and land-cover class and is then applied to the β_0 value. In particular, the correction of an input pixels β^0_{in}, associated to a radar incidence angle $\theta_{i,in}$ and to a specific land-cover class, is performed as:

$$\beta^0_{\theta_{i,ref}} = \beta^0_{\theta_{i,in}} / I(\Delta\theta) \tag{2}$$

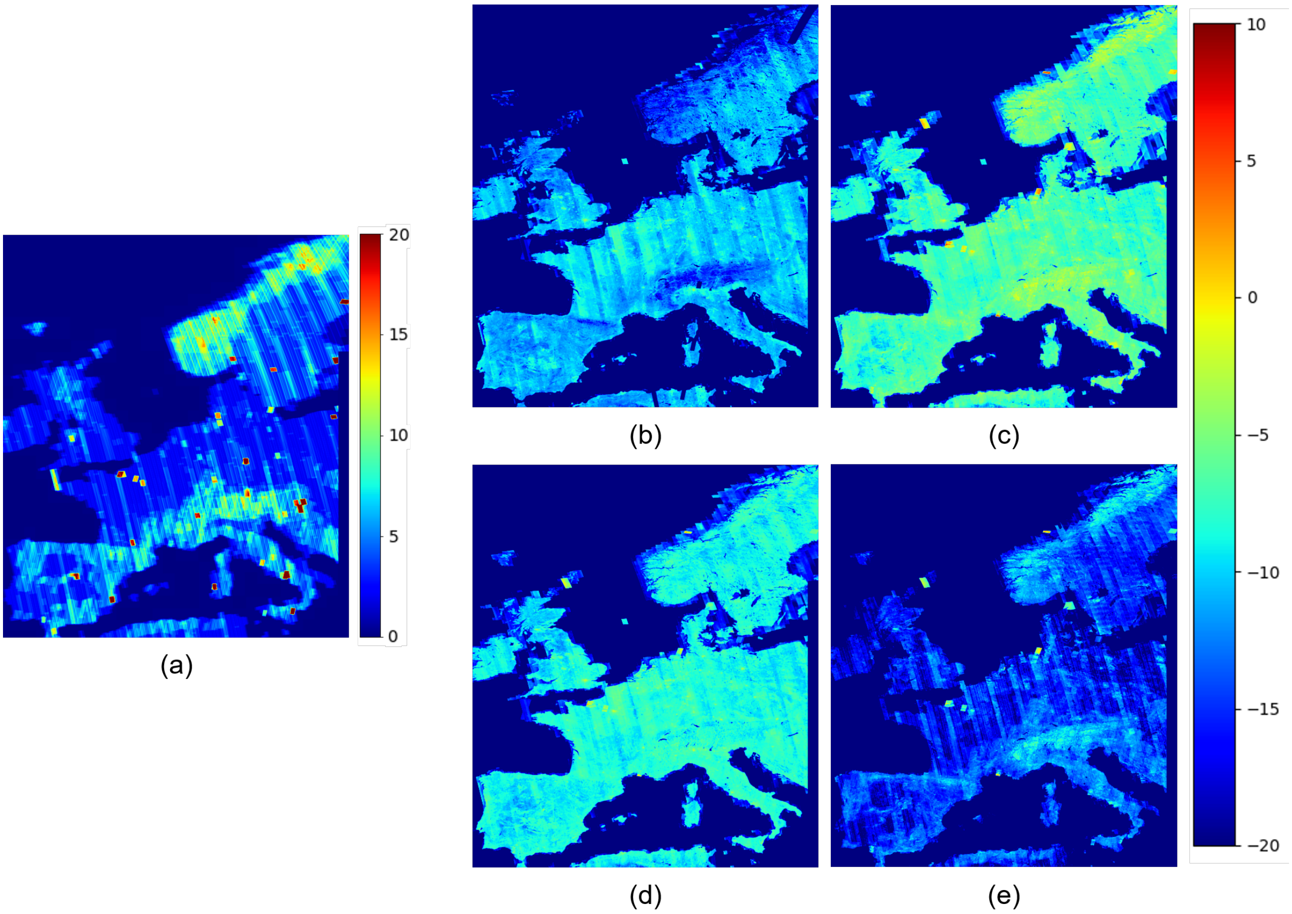

Figure 2 X-band backscatter mosaic over Europe. (a) acquisitions coverage map, (b) backscatter minimum map, (c) backscatter maximum map, (d) backscatter mean map, (e) backscatter standard deviation map. The four backscatter maps on the right are expressed in dB and are referred to HH polarization and 40° output reference radar incidence angle. The maps resolution is the quick-look images one, i.e., $\sim$50 x 50 m^2.

where $\beta^0_{\theta_{i,ref}}$ is the pixel radar brightness of the output cell, I identifies the radar incidence-angle-dependent correction curve associated to a specific land-cover class, while $\Delta\theta$ is defined as:

$$\Delta\theta = \theta_{i,in} - \theta_{i,ref} \tag{3}$$

Note that, doing so, backscatter maps can be generated for any output reference radar incidence angle, starting from the same input data.

Moreover, as introduced in the previous section, the availability of a large amount of SAR data, e.g., several acquisitions over the same ground area at different dates, allows for a statistical analysis of X-band backscatters. Several statistics can be thus derived from the n pixels contributing to the same output cell:

1. backscatter mean value, defined as the average of the n interpolated $\beta^0_{\theta_{i,ref}}$ values;

2. backscatter standard deviation, defined as the sample standard deviation of the n $\beta^0_{\theta_{i,ref}}$ values within the same output resolution cell;

3. backscatter maximum/minimum value, evaluated as the maximum/minimum value of the population of the n interpolated $\beta^0_{\theta_{i,ref}}$ values;

4. backscatter population, defined as the number of input values contributing to the same output resolution cell, i.e., n;

5. backscatter 90^{th}, 95^{th} and 98^{th} percentile, evaluated as the upper/lower bound of the 90%, 95% and 98% distributions of the n interpolated $\beta^0_{\theta_{i,ref}}$ values, respectively.

The above mentioned statistics can be exploited for different purposes. For instance, the mean value can be used for performance estimation, while the standard deviation map can be seen as a measure of the backscatter dynamic and can be therefore used for quantization tasks [9]. Also, the maximum/minimum value can be useful for the evaluation of saturation levels in order to avoid clipping, while the evaluation of the 90^{th}, 95^{th} or 98^{th} percentiles aims to ignore infrequent peaks and thus to give a more reliable estimation of the backscatter distribution.

Given at least the two available global coverages of TanDEM-X, remaining voids represent a very small percentage (less than 0.1%) of all landmasses, thus making an interpolation algorithm for filling the empty output cells almost unnecessary. Moreover, the baseline and side-looking (right/left) flexibility offered by the TanDEM-X mission allowed for the complete acquisition of Antarctica; however, since it is not classified in the *WorldCover 2020* land-cover map, the input quick-look images have not been corrected using the Ulaby backscatter models and the output map has been assumed as the same as the input data.

An example of X-band backscatter mosaic over Europe is shown in Figure 2. It is referred to HH polarization and to 40° output reference radar incidence angle and has been generated with the quick-look images resolution (∼50 x 50 m^2). The maps are the following: Figure 2(a) represents the acquisitions coverage map, while Figure 2(b-e) correspond to the backscatter minimum (b), backscatter maximum (c), backscatter mean (d) and backscatter standard deviation (e) maps, respectively. One can easily note that, despite the availability of a full global dataset, the generation of X-band backscatter maps at very fine resolution (e.g., ∼50 x 50 m^2) has to face to the lack of a large amount of overlapping data, which results in a not reliable estimation of the backscatter distribution. This can be clearly seen in Figure 2(a), where more then 10 acquisitions are available over mountains and forest areas, while only 2 coverages are available over "flat" areas thus making the amount of overlapping data not sufficient for the generation of proper statistical maps. Figure 3 shows a comparison between the backscatter minimum/maximum maps and the 90th lower/upper percentile distributions, respectively. In particular, Figure 3 refers to Germany, only: at the top, the backscatter minimum map (left) and the 90th lower percentile distribution (right) are shown, while at the bottom, the backscatter maximum map (left) and the 90th upper percentile distribution (right) are reported. Note that some outliers are present in the backscatter minimum/maximum maps (especially in the backscatter minimum map, as highlighted in the red box), probably due to some corrupted acquisitions. These ones are removed in the 90th lower/upper percentile distributions, thus giving a more reliable estimation of the backscatter distribution.

As discussed above, the generation of X-band backscatter maps at very fine resolution is not suggested when estimating the backscatter distribution, since several regions do not provide a sufficient number of overlapping data for a statistical analysis. In order to overcome this problem backscatter maps could be generated at coarser resolutions (e.g., few hundreds of meters) in order to extract more reliable statistical maps. Finally, a global X-band backscatter map for HH polarization is currently being processed at ∼500 x 500 m^2 resolution.

3 Performance-Optimized Block-Adaptive Quantization (PO-BAQ)

Performance-optimized block-adaptive quantization (PO-BAQ) [2] is a novel quantization technique aiming at the optimization of the resource allocation of the state-of-the-art quantization algorithm, i.e., BAQ. It was born from the need of handling a large amount of data, in terms of on-board memory and downlink capability, for future SAR systems which will brake the "conventional" limitations of acquiring larger swaths with finer azimuth resolutions. According to this quantization strategy, the bitrate $N_{b,req}$ required for SAR raw data compression can be estimated as:

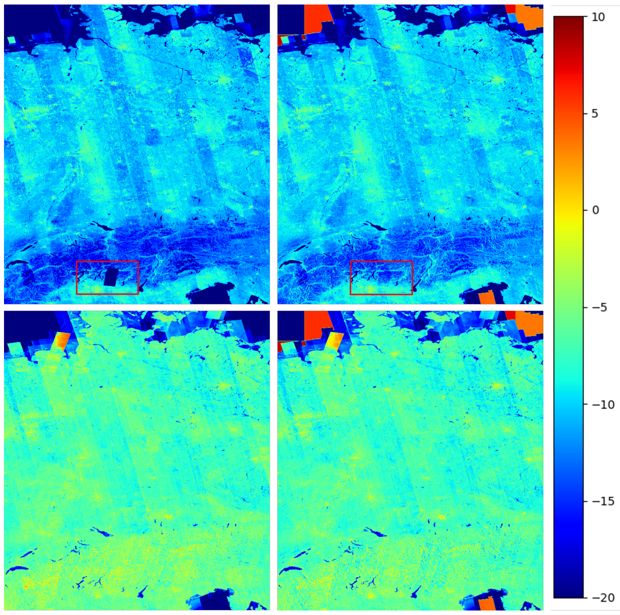

Figure 3 X-band backscatter mosaic over Germany. Top: backscatter minimum map (left) and 90th lower percentile distribution (right). Bottom: backscatter maximum map (left) and 90th upper percentile distribution (right). The four backscatter maps are expressed in dB and are referred to HH polarization and 40° output reference incidence angle. The maps resolution is the quick-look images one, i.e., ∼50 x 50 m^2.

$$N_{b,req} = f(\zeta_{req}, \sigma_{\beta_0}, N_l, N_{acq}). \tag{4}$$

In the equation above, ζ_{req} identifies the requirement imposed on the quantization performance, which can be defined in terms of signal-to-quantization-noise ratio (SQNR), coherence loss or interferometric phase error; N_l is the number of looks, given by the system resolution and the target posting, and N_{acq} is the number of available acquisitions, which is usually defined at mission planning and can be interpreted as a sort of "temporal" looks. Finally, σ_{β_0} represents the local backscatter standard deviation computed over the theoretical integration area of

$$A_{SAR} = L_{chirp} \times L_s; \tag{5}$$

L_{chirp} is the chirp length and L_s is the synthetic aperture of the radar which, in turn, are defined as

$$L_{chirp} = \frac{c\tau_p}{2}, L_s = \lambda\frac{R_0}{L_a}, \tag{6}$$

where c is the speed of light, τ_p stays for the chirp pulse duration, R_0 is the slant range and L_a is the physical antenna dimension along azimuth. The local backscatter standard deviation can be derived from the generated backscatter maps, and in general has to be available a priori before a data take. Moreover, the function *f(.)* in (4) has to be precisely described from a statistical characterization of the performance degradation using real data, as described

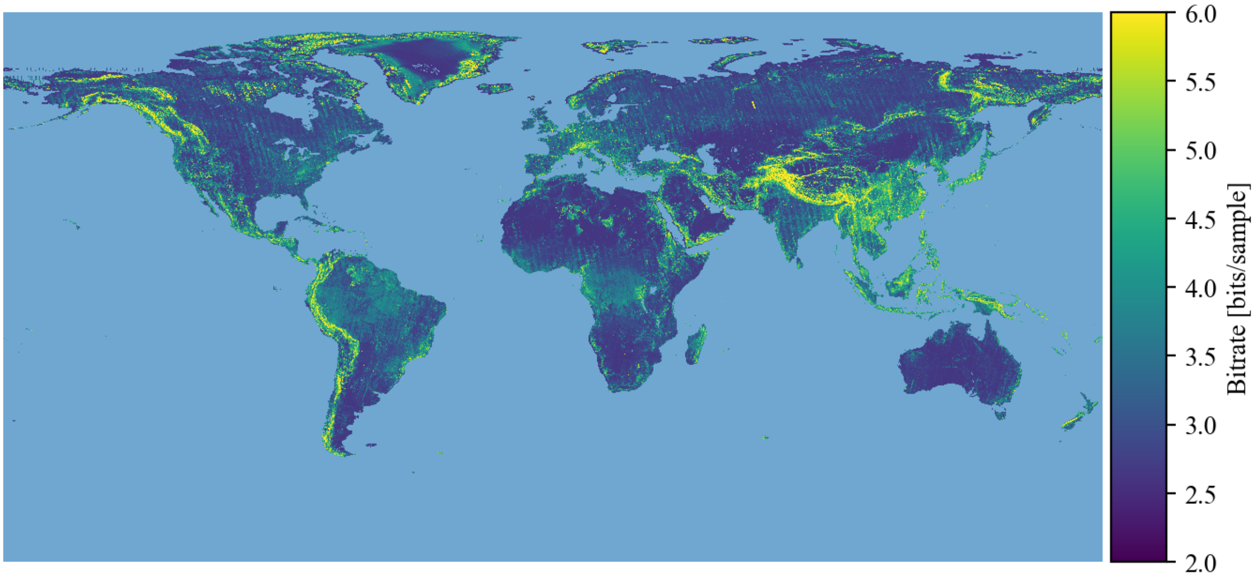

Figure 4 Global bitrate map resulting from a requirement on the interferometric phase error of $\sigma_{\Delta\varphi_q} = 5°$. The bitrate map resolution is about 5 x 5 km^2 at the equator.

in [2]. In particular, it describes the quantization performance degradation as a function of the bitrate N_b and of the backscatter statistics σ_{β_0}. Once all the input parameters and the function *f(.)* in (4) are known, a bitrate map can be derived as

$$N_{b,req} = \underset{N_b \in [N_{b,min}, N_{b,max}]}{\operatorname{argmax}} \{\zeta(N_b, N_l, N_{acq}, \sigma_{\beta_0}) \leq \zeta_{req}\} \tag{7}$$

where $N_{b,min}$ and $N_{b,max}$ are the minimum and maximum allowed bitrates, respectively, which are usually set at system/instrument design level.

As presented in [2], variable bitrate maps can be derived depending on target performance parameters, such as the interferometric phase error or the SQNR. An example of global bitrate map, resulting from a requirement on the interferometric phase error of $\sigma_{\Delta\varphi_q} = 5°$ is shown in Figure 4. As input, a preliminary global X-band backscatter standard deviation map has been used with a resolution of ∼5 x 5 km^2 at the equator, i.e., corresponding to an angular spacing of 0.05° along both latitude and longitude, which provides a reliable statistical measure. Note that a large dispersion in terms of required bitrate is present, ranging from about 2.5 bits/sample to 6 bits/sample.

4 Conclusions

In this paper, the procedure for the generation of global X-band backscatter maps from TDX quick-look images has been discussed. The interpolation approach using the Ulaby models and the newly released *WorldCover 2020* land-cover map has been also presented. Moreover, the benefits of a statistical analysis of X-band SAR backscatters for future SAR systems has been discussed, especially in the field of quantization. A novel PO-BAQ method has been applied as example of novel quantization strategy, in order to point out the importance of a priori knowledge of global backscatter maps for the optimization of future SAR systems. X-band backscatter maps have been generated for HH polarization and with a resolution of ∼50 x 50 m^2, i.e, quick-look images resolution. Thus, the estimation of backscatter distribution has been discussed, focusing mainly on the central role of the output resolution for a reliable statistical analysis. Then, a bitrate map, generated using the proposed PO-BAQ method, has been also presented with a resolution of ∼5 x 5 km^2 at the equator, i.e., corresponding to an angular spacing of 0.05° along both latitude and longitude, showing a large dispersion in terms of required bitrate, ranging from about 2.5 bits/sample to 6 bits/sample. The use of global backscatter maps is in turn an extremely valuable input for a variety of applications, ranging from backscatter statistical analysis to performance optimization, and will further represent a key input for the design of future SAR missions.

5 Literature

[1] P. Rizzoli, B. Brautigam, S. Wollstadt, and J. Mittermayer, “Radar backscatter mapping using TerraSAR-X,” *IEEE Trans. Geosci. Remote Sens.*, vol. 49, no. 10, pp. 3538–3547, 2011.

[2] M. Martone, N. Gollin, P. Rizzoli, and G. Krieger, "Performance-Optimized Quantization for InSAR Applications." *EUSAR 2021; 13th European Conference on Synthetic Aperture Radar*. VDE, 2021.

[3] F. T. Ulaby and M. C. Dobson, *Handbook of Radar Scattering Statistics for Terrain*. Norwood, MA: Artech House, 1989.

[4] D. Small, N. Miranda, and E. Meier, “A revised radiometric normalization standard for SAR,” in *Proc. IGARSS*, Cape Town, South Africa, 2009, pp. IV-

566–IV-569.

[5] T. Fritz, M. Eineder, H. Breit, B. Schättler, E. Boerner, and M. Huber, "The TerraSAR-X basic products—Format and expected performance," presented at the *Eur. Conf. Synthetic Aperture Radar*, Dresden, Germany, 2006.

[6] T. Fritz and M. Eineder, TerraSAR-X Ground Segment Basic Product Specification Document, no. 1.6, Mar. 18, 2009.

[7] GLOBCOVER Products Description Manual. [Online]. Available: http://due.esrin.esa.int/files/GLOBCOVER2009_Validation_Report_2.2.pdf

[8] WORLDCOVER 2020 land cover product. [Online]. Available: https://esa-worldcover.org/en

[9] J. Mittermayer, M. Younis, R. Metzig, S. Wollstadt, J. Márquez, and A. Meta, "TerraSAR-X system performance characterization and verification," *IEEE Trans. Geosci. Remote Sens.*, vol. 48, no. 2, pp. 660–676, Feb. 2010.